THE JOURNAL OF BIOLOGICAL CHEMISTRY
Vol. 277, No. 43, Issue of October 25, pp. 40823–40831, 2002
Printed in U.S.A.

A Key Structural Role for Active Site Type 3 Copper Ions in Human Ceruloplasmin*

Received for publication, July 18, 2002
Published, JBC Papers in Press, August 12, 2002, DOI 10.1074/jbc.M207188200

Patrice Vachette‡§, Enrico Dainese¶, Vadim B. Vasyliev‖, Paolo Di Muro, Mariano Beltramini**, Dmitri I. Svergun‡‡§§, Vincenzo De Filippis¶¶, and Benedetto Salvato****

*From the ‡LURE, Bat. 209d, Université Paris-Sud, B.P. 34, F91898 Orsay Cedex, France, the ¶Department of Biomedical Sciences, University of Teramo, Piazza A. Moro 45, 64100 Teramo, Italy, the ‖Institute for Experimental Medicine, Saint Petersburg 197376, Russia, the **Department of Biology, and CNR Center for Biomedical Technologies, University of Padua, Padua, Italy, ‡‡EMBL, Hamburg Outstation, Notkestraße 85, D-22603 Hamburg, Germany, the §§Institute of Crystallography, Russian Academy of Sciences, Leninsky pr. 59, 117333 Moscow, Russia, and the ¶¶CRIBI Biotechnology Centre, University of Padua, Padua, Italy*

Human ceruloplasmin is a copper containing serum glycoprotein with multiple functions. The crystal structure shows that its six domains are arranged in three pairs with a pseudo-ternary axis. Both the holo and apo forms of human ceruloplasmin were studied by size exclusion chromatography and small angle x-ray scattering in solution. The experimental curve of the holo form displays conspicuous differences with the scattering pattern calculated from the crystal structure. Once the carbohydrate chains and flexible loops not visible in the crystal are accounted for, remaining discrepancies suggest that the central pair of domains may move as a whole with respect to the rest of the molecule. The quasisymmetrical crystal structure therefore appears to be stabilized by crystal packing forces. Upon copper removal, the scattering pattern of human ceruloplasmin exhibits very large differences with that of the holoprotein, which are interpreted in terms of essentially preserved domains freely moving in solution around flexible linkers and exploring an ensemble of open conformations. This model, which is supported by the analysis of domain interfaces, provides a structural explanation for the differences in copper reincorporation into the apoprotein and activity recovery between human ceruloplasmin and two other multicopper oxidases, ascorbate oxidase and laccase. Our results demonstrate that, beyond catalytic activity, the three-copper cluster at the N-terminal-C-terminal interface plays a crucial role in the structural stability of human ceruloplasmin.

Ceruloplasmin (ferro-O_2-oxidoreductase, EC 1.16.3.1) is a circulating copper protein found in vertebrate plasma, which belongs to the family of multicopper oxidases together with ascorbate oxidase and laccases. In humans it accounts for 95% of plasma copper and seems to play an important role in iron metabolism and homeostasis by virtue of its capacity to oxidize Fe^{2+} to Fe^{3+}, which allows the subsequent incorporation of the latter into apotransferrin (1, 2) (for a recent review, see Ref. 3). Mutations in human Cp (hCp),[1] which result in a loss of activity, cause aceruloplasminemia, a neurodegenerative disease whose characterization revealed an essential role for hCp in cellular iron efflux (3, 4). Besides, the protein was shown to exert an antioxidant activity (5) because of its ability to scavenge superoxide radicals (6), a function also strongly dependent on the presence of copper in the hCp molecule (7, 8). More recently, a glutathione-dependent peroxidase activity was detected and associated with a different active site involving Cys-699 (9).

hCp is a single chain of 1046 amino acids (10). It normally binds six copper ions (11), which are classified in three different types according to their spectroscopic properties (12). The x-ray crystallography structure determined at 3.1-Å resolution reveals that the polypeptide chain is folded in six similar domains arranged in three pairs forming a triangular array around a pseudo 3-fold axis (13) (see the schematic diagram in the inset to Fig. 1). The mononuclear type 1 copper sites in domains 4 and 6 involve 2 His, 1 Cys, and 1 Met as copper ligands, whereas in the type 1 site of domain 2 the Met residue is missing. One type 2 copper and the binuclear type 3 copper form a trinuclear cluster binding a dioxygen molecule activated in the peroxide form. The trinuclear cluster is surrounded by four pairs of His residues equally contributed by the N-terminal domain 1 and the C-terminal domain 6, with Cu-N distances of ~2.1 Å. Two residues are bound to the type 2 copper and three residues coordinate each copper atom of type 3 (11, 13).

Recently, the kinetics of CN^--dependent conversion of holo-hCp into the apoprotein were investigated, yielding some insight into the relative affinities of metal ions in the molecule (8). Type 1 and type 2 Cu^{2+} appear to be most sensitive to the treatment, whereas type 3 Cu^{2+} are more tightly bound. Copper-depleted hCp becomes unable both of oxidizing its *in vitro* substrates *p*-phenylenediamine and *o*-dianisidine and of scavenging O_2^- anions. Subsequent copper reincorporation into CN^--treated samples shows that both the final copper content and the recovered enzymatic activity are strongly dependent on the amount of copper left bound to the protein (8). In particular, the removal of type 3 copper ions is essentially irreversible.

* This work was supported in part by the CNRS (to P. V.), RFFI Grants 00-04-49001 and 00-15-97931 (to V. B. V.), the Centro Nazionale della Ricerca/Russian Academy of Medical Sciences Collaborative Program "Copper Proteins and Copper Metabolism" (to E. D., P. D. M., M. B., B. S., and V. B. V.), and by the CNRS/CNR Agreement "Supermolecular Organization and Functional Regulation of Oligomeric Proteins." The costs of publication of this article were defrayed in part by the payment of page charges. This article must therefore be hereby marked "*advertisement*" in accordance with 18 U.S.C. Section 1734 solely to indicate this fact.

§ To whom correspondence should be addressed: LURE, Bat. 209d, Université Paris-Sud, B.P. 34, F91898 Orsay Cedex, France. Tel.: 33-1-64-46-88-55; Fax: 33-1-64-46-41-48; E-mail: patrice.vachette@lure.u-psud.fr.

[1] The abbreviations used are: hCp, human ceruloplasmin; SAXS, small angle X-ray scattering; HPLC, high pressure liquid chromatography; ASA, accessible surface area; AO, ascorbate oxidase; DAM, dummy atom model.

Previous studies, including determination of sedimentation coefficients (14), electrophoretic mobility (15, 16), and spectroscopic analysis using UV absorption, fluorescence, and circular dichroism (CD) (17) indicated that the conformation of apo-hCp is different from that of the holoprotein. The authors of the latter study proposed that upon removal of copper, the protein acquires typical "molten globule" properties, although the presence of a significant fine structure in the near UV CD spectrum and of an efficient tyrosine to tryptophan energy transfer was taken as an indication that the copper-free protein still retains a significant amount of residual tertiary structure (17). In a molten globule state, the secondary structure is largely preserved with concomitant loss of precise side chain packing leading to a less compact conformation exposing hydrophobic moieties to the solvent (18). To characterize further the conformational differences between holo- and apo-hCp, the two protein forms have been studied using size exclusion chromatography and small angle x-ray scattering (SAXS) in solution. The latter method provides information about the global conformation of macromolecules (19), as illustrated by studies of the structural transition of allosteric enzymes (20, 21) or studies of the molten globule state of proteins (22, 23). The results presented here show that hCp undergoes a dramatic structural rearrangement upon copper removal. The SAXS pattern of apo-hCp suggests that the protein explores a large ensemble of open conformations in which the two pairs of domains at each end of the protein, which remained essentially intact, are fairly free to move in solution while still being connected to the central pair by flexible linkers. For the holo form of the protein, indications of rigid body movements of the central pair of domains with respect to the other two domains have been obtained.

EXPERIMENTAL PROCEDURES

Preparation of Holo and Apo-ceruloplasmin—Human holo-hCp was isolated from the pooled sera of healthy individuals following the procedure already described (24). The purity of the preparation was checked spectrophotometrically by measuring the absorbance ratio A_{610}/A_{280} that was ≥0.046, indicating a purity level of at least 95–96%. To prepare the apoprotein, holo-hCp was first fully reduced by dialysis for 2 h against 0.1 M Tris-HCl, pH 7.2, containing 20 mM ascorbic acid and then incubated at 20 °C for 12 h in the presence of CN^- (0.25 mM) and EDTA (10 mM). The reaction was stopped by dialysis against 0.1 M Tris-HCl, pH 7.2 (2 changes for 6 h each). The resulting apoprotein contained less than 1% residual copper as determined by atomic absorption spectroscopy. Protein concentrations were determined spectrophotometrically at 280 nm using a value of 1.61 mg^{-1} cm^2 for the extinction coefficient (25). Absorption spectra were determined using a Hewlett-Packard model HP 8452A spectrophotometer.

Hydrodynamic Measurements—Gel filtration chromatography was carried out on a TSK G3000SW analytical column (7.5 × 600 mm) eluted at a constant flow rate of 0.3 ml min^{-1} with 25 mM Tris-HCl buffer, pH 7.5, containing 0.15 M NaCl. The absorbance of the effluent was recorded at 226 nm. Typically, 20–50 μg (10–25 μl) of holo- and apo-hCp in the same elution buffer were loaded onto the column by using a Rheodine model 8125 valve connected to a PerkinElmer Life Sciences HPLC system, model 410-BIO. Chromatographic data were collected and processed using the CHROM3 software run on a 7700 professional computer.

SAXS Data Recording and Analysis—SAXS measurements were performed on the small angle x-ray scattering instrument D24 at LURE using synchrotron radiation from a bending magnet of the storage ring DCI. The instrument, the data acquisition system (26), and the evacuated cell (27) have already been described. The wavelength of the monochromatic ($\Delta\lambda/\lambda = 10^{-3}$) x-ray beam was adjusted to 1.488 Å (absorption K-edge of Ni). All samples were measured in 0.1 M Tris-HCl buffer, pH 7.2. To ensure the monodispersity of the samples for R_g determination, a solution of holo (respectively, apo)-hCp was loaded onto a size exclusion (SE) HPLC column and eluted in the above buffer. The top fraction of the peak corresponding to monomeric hCp was collected and immediately examined by SAXS. The protein concentration of each fraction was in the range of 1 to 3 mg ml^{-1}. Wide angle data are weak but much less sensitive to the presence of a small amount of oligomer. They were recorded using solutions at a concentration of 125 mg ml^{-1} (holo-hCp) and 45 mg ml^{-1} (apo-hCp). The radius of gyration (R_g) was determined using the Guinier approximation (28): $I(s) = I(0)\cdot\exp((-4\pi^2/3)R_g^2 s^2)$, where I(0) is the scattering intensity at zero scattering angle. I(0)/*c* is proportional to the molecular weight of the protein.

The complete scattering curves used for further analysis were obtained by splicing small angle, low concentration data with the wide angle, high concentration curve after proper scaling. The distance distribution function $p(r)$ corresponds to the distribution of distances between any 2 volume elements within one particle. It has been determined using the indirect Fourier transform method as implemented in the program GNOM (29). This function provides an estimate of the radius of gyration derived through the following relationship.

$$R_g^2 = \frac{\int r^2 p(r) dr}{2\int p(r) dr} \qquad \text{(Eq. 1)}$$

Shape Determination—The *ab initio* shape determination was performed using the dummy atom model (DAM) method (30) as implemented in the program DAMMIN. A sphere of diameter D_{max} is filled by densely packed small spheres (dummy atoms) of radius $r_0 \ll D_{max}$. The DAM structure is defined by a configuration vector X assigning an index to each atom corresponding to solvent (0) or solute particle (1). In keeping with the low resolution of the solution scattering data, the method starts from a random configuration and searches for a configuration *X* minimizing $f(X) = \chi^2 + \alpha P(X)$, where $\alpha > 0$ is a positive parameter and the penalty term $P(X)$ ensures that the DAM has low resolution with respect to the packing radius r_0. To remove the scattering contribution because of the internal fluctuations undesirable for the shape analysis, a constant was subtracted from the experimental data to ensure that the intensity decays as s^{-4} following Porod's law (31) for homogeneous particles. This procedure yields an approximation of the shape scattering curve (*i.e.* the scattering because of the excluded volume of the particle filled by constant density) and this data is used in the *ab initio* analysis.

Calculation of Scattering Patterns from Crystal Coordinates—The atomic coordinates of the holo-hCp were taken from the Protein Data Bank (32) and are available in the Research Collaboratory for Structural Bioinformatics Protein Data bank (13), entry 1kcw. The scattering from the crystallographic structure was calculated using the program CRYSOL (33), which takes the scattering from the solvation shell into account and fits the experimental scattering curve using two adjustable parameters, the excluded volume of the particle and the contrast of the hydration layer $\delta\rho_b = \rho_b - \rho_s$, (here, ρ_s and ρ_b denote the scattering length densities of the bulk and bound solvent, respectively). The values of $\delta\rho_b$ found for models of the holo and apo conformations ranged from 0.02 to 0.04 el. $Å^{-3}$, values commonly encountered with other proteins. The structure is not complete, because three external loops corresponding to residues 339–346, 475–482, and 885–891 could not be resolved in the structure any more than the 6 C-terminal residues. This is most likely because of a great mobility of these parts of the molecule that cancelled out their contribution to the diffraction intensities, making them invisible to x-rays as it were. Because they are very mobile, their precise conformation and location is not a critical issue, and certainly not when it comes to determining their contribution to the SAXS pattern, *i.e.* at low resolution. Therefore, these missing parts were modeled using the software Turbo-FRODO (34) and the scattering pattern calculated and fitted against the experimental curve of the holo-hCp.

Carbohydrate Chain Modeling in Holo-hCp—The complete sequence of the carbohydrate chains are reported by Rydèn (35). As can be seen in Table I, they comprise one biantennary oligosaccharide constituting two of three chains and a triantennary oligosaccharide constituting the third of the three chains observed on average on the molecule of hCp. However, hCp is heterogeneous in the degree of glycosylation, which varies from two to four chains per protein molecule (35). Finally, the biantennary or the larger triantennary oligosaccharide can be found attached at the same site, implying that a microheterogeneity also exists at this level. The three-dimensional structure of a fragment of carbohydrate chain containing nine hexose units bound to a protein was found in the structure of an Fc fragment (36) (Protein Data Bank entry 1fc1). The missing terminal sialic acid was found in a structure of influenza virus neuraminidase (37) (Protein Data Bank entry 2qwb). The complete biantennary and triantennary chains were built using

TABLE I
Structure of the oligosaccharide chains of hCP: (a) biantennary oligosaccharide and (b) triantennary oligosaccharide (35)

(a)

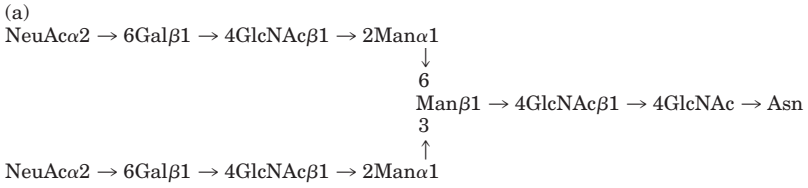

(b)

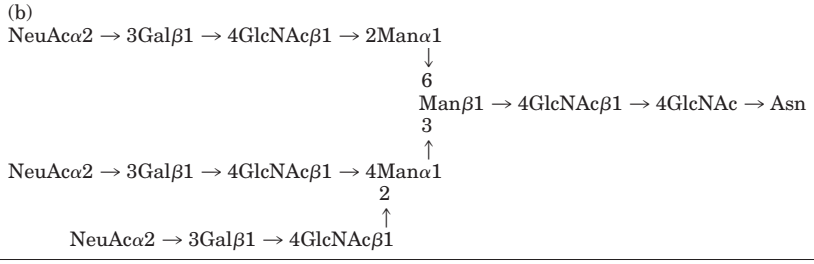

Turbo-FRODO. No particular care was taken during the process to respect a precise stereochemistry of the sugar chains thus built, because this is of no consequence on the resulting scattering pattern, which only depends on the general position of the chain with respect to the protein. The same program was used to add the various chains to the glycosylation sites. The chains were placed in an arbitrary position well exposed to the solvent, because their high mobility makes them likely to explore a fairly large volume around the attachment site with no privileged orientation or position. Their contribution to the scattering is thus that of an average conformation. Molecules with one triantennary chain and from one to three biantennary oligosaccharides were obtained in this way and used for calculations.

Apo-hCp Modeling—Modeling the apo-hCp involved two successive steps starting from the model of the holoprotein complete with loops, C-terminal end, and three carbohydrate chains. The first step made use of the program Turbo-FRODO already mentioned to create extended conformations of the molecule. The central pair of domains was kept fixed during the whole process and considered as associated with the coordinate frame. The three domain pairs are defined as follows: domain {1,2} amino acid residues 1–338; domain {3,4} amino acid residues 339–702; domain {5,6} amino acid residues 703–1046. The domain pair {5,6} was rotated around an axis parallel to the *y axis* of the coordinate frame passing through the N(H) of residue 703, whereas domain pair {1,2} was rotated around an axis parallel to the *x axis* passing through the C(O) atom of residue 338. These rotations were a simple means of describing rigid body movements of the domains around one extremity of the linker connecting them to the central domain. The second step of the model search made use of the program ASSA (38) running on an SGI Indigo^2 work station. As input, the program uses the atomic coordinate files of proteins in PDB format and the scattering amplitudes of the corresponding protein calculated using CRYSOL. Given two such proteins and the experimental scattering pattern of the (1:1) complex between them, their mutual position and orientation can be interactively optimized so as to fit the scattering data. In the specific case of the apo-hCp, the protein was divided in two parts: the first one comprising the pairs of domains {1,2} and {3,4} was kept fixed, whereas the position and orientation of {5,6} was adjusted. Here again, only rotations around the Cα of residue 703 were considered, so as to allow for rigid body movements of {5,6} without disrupting the main chain connectivity. In a second run, the roles of protein domains {1,2} and {5,6} were exchanged and the process was repeated. No further refinement was required.

Analysis of Domain Interfaces—Domain interfaces have been analyzed using the Protein-Protein Interaction Server by J. Thornton and S. Jones ((39), available at www.biochem.ucl.ac.uk/bsm/PP/server/index.html). For ascorbate oxidase (AO) only monomer A was considered (40), Protein Data Bank entry 1a02. Atomic coordinates for laccase are also available from the Protein Data Bank, entry 1a65 (41). Among the various parameters characterizing the interface that are returned by the program, we have considered here the number of hydrogen bonds, the accessible surface area (ASA), the gap volume calculated, and the gap index. The accessible surface area is calculated using the Lee and Richards algorithm (42) and is defined as the surface mapped out by the center of a probe sphere of radius 1.4 Å rolled around the van der Waals surface of the protein. For a given interface, the value is calculated for each partner in isolation and within the complex before computing the difference. The value of the interface ASA given in Table II is the sum of the differences for both partners. The gap volume between the two interacting domains is calculated using the program SURFNET (43). Finally, the gap index is defined as the ratio of the gap volume to the interface ASA. This index is a measure of the complementarity of the interacting surfaces. Its mean value over a panel of homodimers and heterocomplexes is 2.20 (respectively, 2.48) with a standard deviation of 0.87 (1.02) and maximal values of 4.43 (5.17) (39).

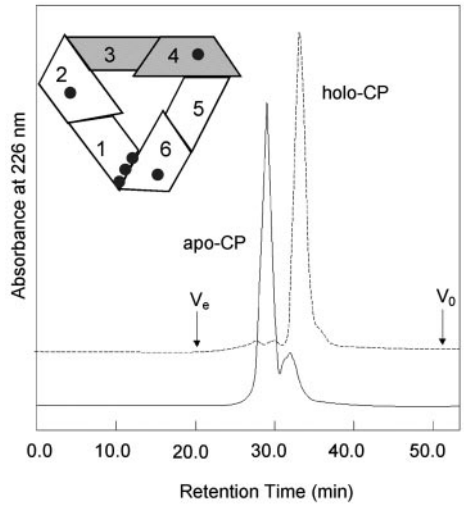

FIG. 1. **HPLC gel filtration chromatography of holo (*dashed line*) and apo (*solid line*)-hCp in 25 mM Tris-HCl buffer, pH 7.5, containing 0.15 M NaCl.** The profile of holo-hCp is shifted along the *y axis* for the sake of clarity. V_e and V_0 denote the position of excluded and included volumes, respectively. See "Experimental Procedures" for details. In the *upper left corner*, schematic diagram of hCp (11). The domains are sequentially numbered from the N- to the C-end, with the central pair {3,4} *underlined* with a *gray shading*. Copper atoms are displayed as *dark circles*.

Rigid Body Movement in Holo-hCp—The position of the central pair of domain with respect to the other two pairs was optimized using the refinement routine included in the program MASSHA (44). This routine explores all six translational and rotational parameters to optimize the fit of the calculated pattern to the experimental scattering curve.

RESULTS

Gel Filtration Experiments—The results of analytical gel filtration, reported in Fig. 1, provide evidence that apo-hCp has a larger hydrodynamic volume as compared with that of the holoprotein, indicating that removal of copper ions leads to a more expanded structure. This observation is consistent with the results of a previous comparison of the physicochemical

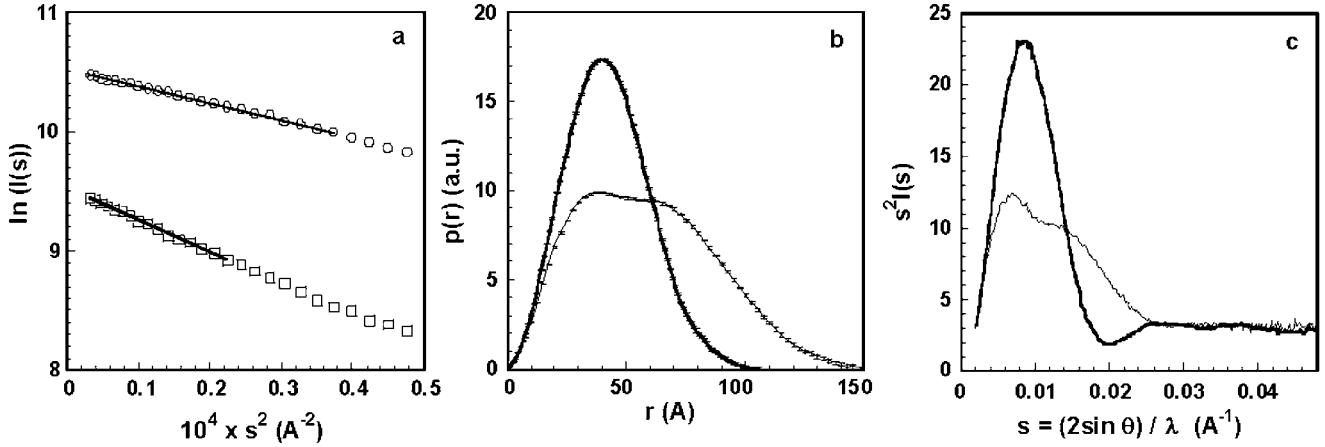

FIG. 2. **Analysis of the SAXS patterns of holo (*circles* and *thick lines*) and apo (*squares* and *thin lines*)-hCp.** *a*, Guinier plots. The concentrations of the solutions used were 2.1 mg ml^{-1} (holo, *top curve*) and 1.6 mg ml^{-1} (apo, *bottom curve*). The *straight lines* result from the linear fit to the data. The curve of holo-hCp has been displaced up the vertical axis by 1 ln unit for the sake of clarity. *b*, distance distribution functions p(*r*). The functions are normalized to the integrated value, *i.e.* to I(0)/*c*, which is proportional to the molecular weight. *c*, Kratky plots normalized to I(0)/*c*.

characteristics of the holo and apo forms indicating that copper depletion induces a conformational change interpreted at the time as possibly leading to the molten globule state (17). The second, minor peak on the low molecular weight side of the apo-hCp elution profile is most likely because of some limited proteolysis, suggesting a greater sensitivity of the protein after copper extraction. This had already been suggested by the marked difference in half-life between circulating hCp in the holo form (5.5 days) (45) and the apo form with a much shorter half-life of about 5 h (46).

Integral Parameters from SAXS Measurements—The radius of gyration of hCp in the holo and apo forms was calculated using the Guinier approximation from the range of scattering vectors within $2\pi sRg < 1.3$ (31) (Fig. 2*a*). The concentrations (*c*) were sufficiently low to make interparticle interactions negligible in the buffer used. The R_g values derived from the Guinier analysis are 32.5 ± 0.5 and 45.2 ± 0.5 Å for the holo- and apo-hCp, respectively. The values of I(0)/*c* for various samples of holo- and apo-hCp were identical within experimental error, as expected for two proteins with the same molecular mass, showing that the apo-hCp solution used for SAXS experiments was free from protein degradation.

Further analysis was performed in terms of the distance distribution function *p*(*r*) (Fig. 2*b*) determined for holo- and apo-hCp as described under "Experimental Procedures." Their qualitative comparison suggests that the conformation of the holo-hCp is globular (p(*r*) is essentially symmetric with respect to the most frequent distance), whereas that of the apo-hCp is rather anisometric. Quantitatively, the maximum dimension of the holo form D_{max} is equal to 110 ± 5 Å, whereas the apo form is significantly larger (D_{max} = 155 ± 5 Å). The radii of gyration of the two forms, calculated from the p(*r*) functions are 32.3 ± 0.2 and 45.9 ± 0.3 Å, respectively, in good agreement with those determined using the Guinier approximation.

A sensitive probe of the compactness of a particle is provided by the so-called Kratky plot $s^2I(s)$ *versus* *s* (31). Indeed, for a Gaussian polymer chain, the scattering profile at high angles varies like s^{-2} instead of the s^{-4} behavior of the Porod law for globular objects (31). This marked difference in the asymptotic behavior is most conveniently examined using the Kratky plot: the scattering curve of a globular particle will present a distinctive bell-shaped curve, whereas the curve of a Gaussian chain displays a plateau. The two Kratky plots for holo- and apo-hCp are presented in Fig. 2*c*, where the intensities have been scaled to protein concentration. It can be seen that the holo- to apo-hCp transition does not result in a complete loss of globular structure: the apo-hCp still presents a clear maximum, although of different shape and intensity. The maximum is shifted toward small angles, in agreement with the observed increase in the value of the radius of gyration, whereas the integrated intensity for the apo-hCp in the range of the maximum (0.0045 $Å^{-1} \leq s \leq 0.014$ $Å^{-1}$) only amounts to 60% of the corresponding value for the holoprotein, indicating that the removal of copper decreases the compactness of the molecule. In summary, the comparison between the integral parameters of the holo and apo forms of hCp shows that upon copper removal, hCp undergoes a major conformation change toward a more extended shape indicated by a 40% increase in the values of both the radius of gyration and the maximum diameter of the protein.

Conformation of Holo-hCp in Solution—The scattering pattern of the crystal structure of holo-hCp was calculated using the program CRYSOL and is shown in Fig. 3*a* (*thin black line*) together with the experimental pattern (*blue dots* with *error bars*). The two curves display noticeable differences, beyond any experimental or computing error, most remarkably in the small angle region and around the first subsidiary minimum and maximum. The radius of gyration and the maximal diameter computed from the crystallographic model (30.0 and 85 Å, respectively) are significantly smaller than the experimental values. The first minimum and maximum on the calculated pattern are much sharper than the experimental ones, the minimum is shifted toward smaller *s* values, and the oscillations observed in the *s* range [0.028 $Å^{-1}$, 0.045 $Å^{-1}$] are barely detectable in the experimental pattern. Taking into account the pseudo 3-fold symmetry of the molecule, the experimentally observed weaker modulation suggests that, in solution, there is some departure from the symmetry observed in the crystal structure.

Differences between the crystal structure and the conformation in solution have already been observed (21, 47, 48) that have been attributed to the effect of packing forces in the crystal. However, before considering the possible effect of the crystal lattice on the structure of hCp, one should remember that hCp is a glycoprotein with four sites of *N*-glycosylation (35). Of these four sites, one, at Asn-743, shows no trace of the bound carbohydrate chain in the electron density, two at Asn-339 and -378 only show the first *N*-acetylglucosamine residue, whereas two residues have been placed for Asn-119 (11). These carbohydrate chains are located on the surface of the protein,

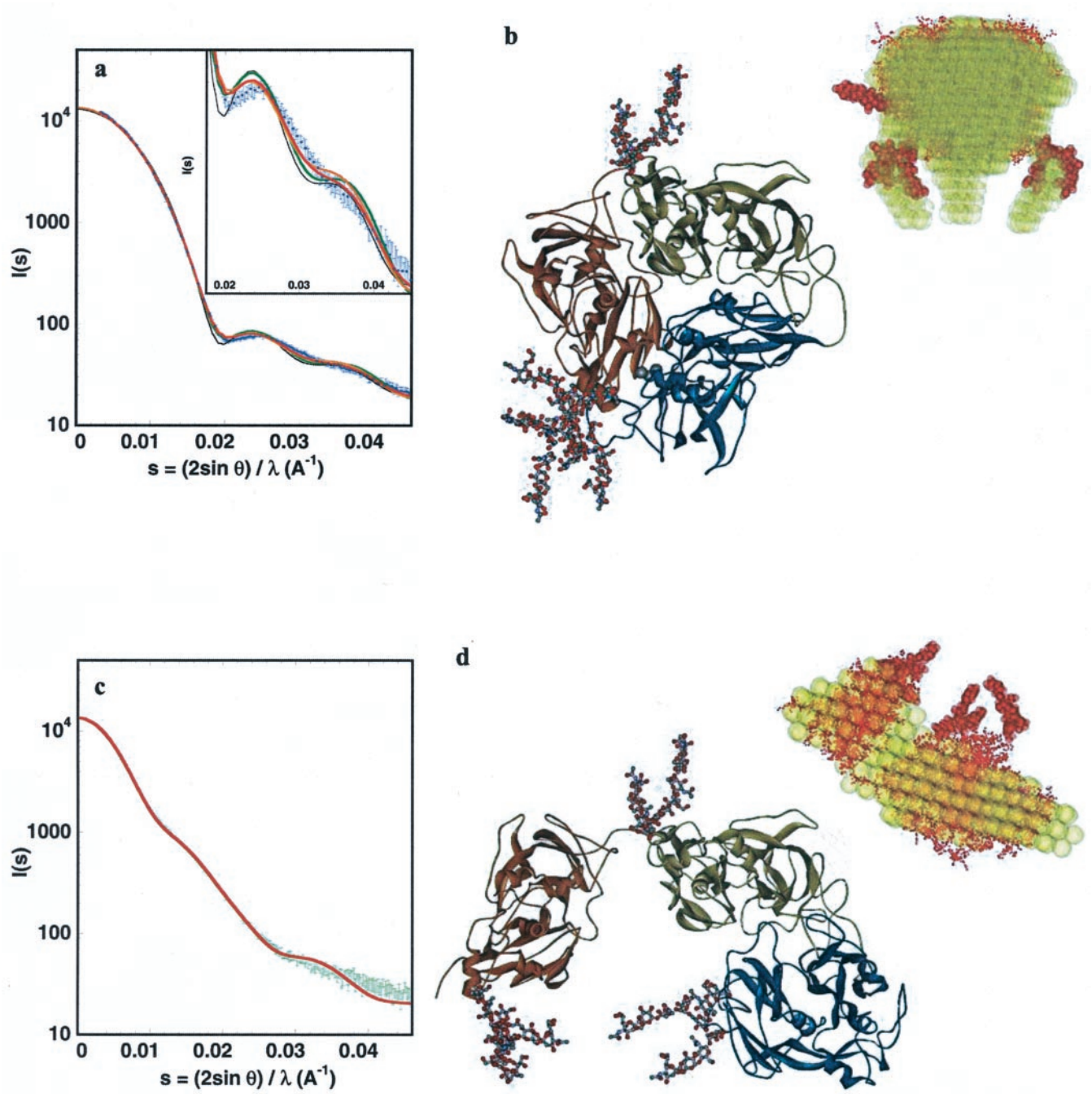

FIG. 3. **Modeling holo- and apo-hCp.** *a*, experimental and calculated curves of the holo form: *blue dots with error bars*, experimental data; *thin black line*, calculated curve of the completed crystal structure with no sugar chain added; *green line*, calculated curve of the protein with three sugar chains. *Light brown line*, calculated curve of the glycosylated model after refinement of the position of the central pair of domains. *Red line*, calculated curve of the glycosylated model after refinement of the position of the central pair of domains from a different starting position. *Inset*, magnification of the outer region of the holo curves. *b*, the structure of the holoprotein in *ribbon* representation, with the attached carbohydrate chains shown in *ball* and *stick* representation, is viewed along the pseudo 3-fold axis. The first pair of domains {1,2} is shown in *copper*, the second {3,4} in *gold*, the last pair {5,6} in *blue*. The *inset* shows an orthogonal view of the molecule (*red* markers for the protein moiety, red CPK for the sugar chains) superimposed on the *ab initio* model determined by DAMMIN (*yellow semi-transparent spheres*). *c*, experimental and calculated curves of the apo form: *green dots with error bars*, experimental data; *red line*, calculated pattern of the refined model of the glycosylated apoprotein. *d*, the structure of the apoprotein in *ribbon* representation, with the attached carbohydrate chains shown in *ball* and *stick* representation, is viewed along the pseudo 3-fold axis. Color code for domains as in *b*. The *inset* shows an orthogonal view of the molecule (*red markers* for the protein moiety, *red CPK* for the sugar chains) superimposed on the *ab initio* model determined by DAMMIN (*yellow semi-transparent spheres*). The *ribbon*, *ball* and *stick*, and CPK representations have been obtained using the program WebLab ViewerLite37™ (Molecular Simulations Inc.).

mostly exposed to the solvent, and will significantly contribute to scattering in the small angle range, thereby increasing the value of the radius of gyration. Furthermore, these chains will decrease the pseudo 3-fold symmetry for three reasons: (i) the glycosylation sites do not obey the symmetry; (ii) hCp presents a marked heterogeneity in the degree of glycosylation, from two to four carbohydrate chains per protein molecule, whereas bi-antennary or the larger triantennary oligosaccharides could be found at the same site (35); (iii) these carbohydrate chains move in the solvent around their binding site. This assertion is supported by the nearly complete absence of sugars from the electron density map, although no attempt had been made to

cleave the sugar chains off from the protein before crystallization.[2] Therefore, it appears that the contribution of the glycans could account for the two main discrepancies between the calculated and the experimental patterns, a larger experimental value of the radius of gyration and of the maximal diameter and a lower apparent degree of symmetry.

To test this hypothesis, the carbohydrate chains were modeled as explained under "Experimental Procedures" and the glycoprotein scattering pattern was calculated using CRYSOL. The resulting model with three sugar chains, the average chain number, is presented in Fig. 3*b*, whereas the corresponding curve is shown in *green* in Fig. 3*a*. The agreement with the experimental curve is much improved, the value of the radius of gyration (32.0 Å) nearly coincides with the experimental one and the first minimum is essentially identical in depth and position to that in the experimental curve. The curve calculated with four sugar chains is very similar with only a small increase in the value of the radius of gyration, whereas that with one chain is closer to the curve of the unglycosylated protein (data not shown). Therefore, we consider that the sugar chains do account for most of the observed differences. However, even the curve calculated with all four sugars displays the same oscillations at higher angles with barely reduced amplitudes as compared with the curve of the unglycosylated protein. A proposal to account for these residual differences will be presented further below.

In parallel to the above modeling, *ab initio* calculations of the overall shape of the molecule from the SAXS pattern were performed using the program DAMMIN (30). To constrain the calculations, conditions of oblateness and 3-fold symmetry of the particle shape were imposed. Several independent reconstructions obtained from randomly generated starting configurations yielded consistently characteristic shapes with three extensions protruding from the core of the molecule, the size of which is comparable with the length of the carbohydrate chains. The calculated patterns are nearly identical to the experimental curve after subtraction of a constant value (see "Experimental Procedures"). The DAMMIN model is shown in the *inset* to Fig. 3*b* together with the superimposed crystal structure complete with sugar chains. The similarity is striking, and all the more so if one considers that the 3-fold symmetry imposed in the DAMMIN calculation is not obeyed by the sugar chains. Indeed, two glycan chains are rather well superimposed with two of the three protrusions, the distance between which neatly fits the average distance between the chains bound at Asn-378 and Asn-743. This agreement constitutes a further argument in support of our model for holo-hCp, as well as a testimony to the potential of the *ab initio* approach.

Conformation of Apo-hCp in Solution—A difference close to 40% in the radius of gyration between the holo and apo forms of hCp clearly indicates that copper removal causes a dramatic change in the conformation of the protein. A comparison of the scattering patterns from the two forms in Fig. 2*c* shows that in the small angle range, corresponding to s values lower than 0.026 $Å^{-1}$, the two patterns bear no similarity whatsoever, whereas at larger s values they are practically identical within experimental error. The scattered intensity in the innermost region of the curve, corresponding to large distances, is determined by the mutual arrangement of the domains. In contrast, the scattered intensity in the latter range is because of interference between scatterers at distances smaller than 40 Å, with a strong contribution from intradomain distances. These considerations suggest that upon copper removal, the domains remain essentially intact whereas their relative positions are thoroughly modified.

The low resolution shape of the apo form reconstructed *ab initio* from the scattering data gave us a first hint to the possible domain rearrangements. Attempts at imposing a 3-fold symmetry led to physically unreasonable flat structures indicating that this symmetry is not maintained in the apo form of hCp. The low resolution model of the protein restored without the symmetry restrictions is presented in the *inset* to Fig. 3*d* (*yellow semi-transparent spheres*). The calculated curve is undistinguishable from the experimental data after subtraction of a constant value. Several independent reconstructions yielded very similar shapes suggesting that the domains in the apo-hCp are in a more open arrangement than the triangular array observed in the holo form, the symmetry of which cannot be preserved. This is easily rationalized when one takes into account the specific distribution of copper within the molecule. Indeed, half of the copper content is found in the trinuclear site coordinated to histidine side chains contributed by both the N-terminal and C-terminal domains. It is conceivable that these coordinate bonds that link together domains 1 and 6 contribute to the stability of the interface to the extent that their suppression upon copper removal leads to the loss of the interface. Each of the pairs {1,2} and {5,6} of domains could then leave its position in the holoprotein and, because it is connected to the central pair {3,4} by a flexible linker, freely move in solution, leading to a more extended conformation for the whole apomolecule, in qualitative agreement with our SAXS observations.

Based on the low resolution shape and on previous considerations, models were created using Turbo-FRODO (see "Experimental Procedures") and the calculated scattering curves were compared with the experimental pattern of the apo molecule. Several patterns displayed a global trend similar to that of the experimental curve. The best model was then further refined using the program ASSA (38). The resulting pattern is shown in Fig. 3*c* together with the experimental pattern of the apo-hCp, and the model is presented in Fig. 3*d*. The agreement appears to be excellent over the whole angular range, corresponding to almost 3 orders of magnitude in intensity. However, the value of the radius of gyration, derived from the very small angle region, is about 43.3 Å, close to but significantly smaller than the experimental value. This observation does not invalidate the result of our approach, which does not postulate a unique structure for the apo form of hCp. Indeed, the starting point of our analysis is that the domains, connected by flexible linkers, become loose and move essentially freely in the absence of copper. This flexibility is already apparent in the crystal structure of the holoprotein, because residues 339–346 between domains {1,2} and {3,4} are not located in the electron density map nor residues 885–891 between domain 5 and domain 6, whereas residues 700–702 between domains {3,4} and {5,6}, although positioned in the structure, present very high values of the thermal agitation factor B suggestive of a great mobility. Therefore, the apo form of hCp does not possess a unique conformation in solution but explores a large conformational space essentially described by the mutual rigid body movements of the domains considered in the modeling process. The resulting curve is an average of all accessible conformations weighted by their respective fractional concentration. The lower value of the radius of gyration found upon refinement suggests that there exists no single conformation, the scattering curve of which is identical to the experimental average pattern. Restricting the fitting range to the central part of the pattern leads to more open structures than that shown in Fig. 3*d*, with the same value of the radius of gyration than the experimental one, at the expense of a worsened global fit. No other information on the distribution of the accessible confor-

[2] P. Lindley, personal communication.

TABLE II
Interface parameters obtained from the Protein-Protein Interaction Server (39) for hCp, ascorbate oxidase, and laccase

	hCp (1kcw.pdb)	Ascorbate oxidase (1a02.pdb, monomer A)	Laccase (1a65.pdb)
Interface 1–2 (1–3,1–4,2–3,2–4) for hCp			
Number of H-bonds	2 + 1 + 2 + 2 = 7	30	19
ASA[a] (Å^2)	453 + 204 + 985 + 2018 = 3660	3392	3139
Gap index[b] (Å)	3.45/13.9/5.13/4.05	1.3	1.0
S-S bond	0	1	1
Interface 2–3 (3–5,3–6,4–5,4–6) for hCp			
Number of H-bonds	0 + 0 + 12 + 2 = 14	32	21
ASA[a] (Å^2)	0 + 0 + 1684 + 1010 = 2694	4625	2505
Gap index[b] (Å)	na/na/3.0/5.95	1.4	1.7
S-S bond	0	0	0
Interface 1–3 (1–5,1–6,2–5,2–6) for hCp			
Number of H-bonds	2 + 3 + 2 + 11 = 18	10	14
ASA[a] (Å^2)	538 + 956 + 269 + 2243 = 4006	2482	3424
Gap index[b] (Å)	3.15/6.0/18.5/3.3	2.2	1.9
S-S bond	0	1	1
Intra-pair interfaces in hCp	1–2	3–4	5–6
Number of H-bonds	50	46	22
ASA[a] (Å^2)	7632	7971	5351
Gap index[b] (Å)	0.79	0.74	1.09
S-S bond	0	0	0

[a] Accessible surface area.
[b] For definition, see under "Experimental Procedures."

mations is available, and it can only be surmised, on the basis of the proposed structure, that it is likely to be fairly broad, the domain orientations and positions being only restricted by the presence of the other two domains and the length of the linkers. Finally, the averaging of all curves associated with the broad distribution of accessible conformations explains the absence in the experimental data of any oscillation at $s > 0.03$ Å^{-1}.

DISCUSSION

The Model for Apo-hCp—Despite its success in accounting very economically for the dramatic change in the scattering pattern of hCp associated with copper removal, our model might meet with some skepticism raised by its basic assumption that all three interfaces are totally disrupted in the apo form. Indeed, it may seem *a priori* unlikely that these interfaces could disappear altogether so easily, all the more so that the corresponding interfaces and the global conformation have been reported to be hardly affected by copper removal in the case of AO and laccase, two other members of the multicopper oxidase family whose crystal structures have been determined at high resolution (40, 41). These two proteins possess, like hCp, a trinuclear copper cluster located between domains 1 and 3 (they comprise 3 instead of 6 domains) that equally contribute the coordinating His residues.

To get some insight into this issue, the interfaces between domains of all three proteins were systematically analyzed using the Protein-Protein Interaction Server by J. Thornton and S. Jones (39). For hCp, interfaces between domains within a pair, {1,2}{3,4}{5,6}, were also studied to provide an internal comparison. The values of several parameters describing the domain interfaces are presented in Table II. First, the values of ASA (see "Experimental Procedures") are similar for all three proteins when the pairs of domains in hCp are considered, although they display large variations at the level of individual domains. Interfaces between domains within a pair display ASA values approximately two to four times as large as the most extensive area between domains from different pairs (Table II, bottom row). Second, the number of hydrogen bonds for hCp is smaller or equivalent to that observed in AO or laccase although they involve pairs of domains instead of single domains. Third, a measure of the shape complementarity of the interacting surfaces is provided by the gap index (see "Experimental Procedures"). Whereas values between 1.0 and 2.2 for the various interfaces of AO and laccase are indicative of tight interfaces, the values for the hCp interfaces are most contrasted: interfaces within pairs of domains display the lowest of all values, between 0.74 and 1.09, indicating a very high level of surface complementarity and supporting the view of holo-hCp as a trimer of very tight pairs of domains, whereas the interfaces between domains from different pairs have values ranging between 3 and 6 for the more extensive ones, suggesting a low level of shape complementarity between opposing surfaces. This is likely associated with the presence of interstitial water at most interfaces that would reduce the energetic cost accompanying the solvent exposure of hidden surfaces following copper removal. Finally and most importantly, two disulfide covalent bridges at the {1,2} and {1,3} interfaces are present in AO and laccase that will keep the domains together. None is observed in the case of hCp.

Relevant information can also be found in studies of the functional and structural effect of copper removal performed for all three proteins. AO can be fully depleted from copper using a CN^- treatment similar to that used here for hCp, and the protein can be reversibly reconstituted with complete recovery of enzymatic activity (49). Furthermore, a systematic analysis of the effect of copper depletion on the sensitivity of AO to thermal and chemical denaturation concluded that copper affects the stability but not the protein conformation (50). Similar observations have been made with laccases, which almost completely regains the activity, copper content, and spectroscopic properties of the native protein upon treatment of the apoprotein with cuprous ion (51, 52). In contrast, apo-hCp, fully depleted from its copper atoms as studied here, is unable to recover its copper complement and its enzymatic activity (8). In particular, the two type 3 copper atoms, which are the most resistant to CN^- treatment and require the preliminary reduction of Cu^{2+} to Cu^+ with ascorbate for removal, can never rebind, suggesting that the binding site is not available any more (8).

All these observations, both structural and functional, build a strong body of evidence showing that the interactions be-

tween the pairs of domains in hCp are significantly weaker than the domain interactions in AO and laccase. They fully support our proposal that all three interfaces in hCp are disrupted upon loss of the trinuclear site at the Nter-Cter interface. Complementary observations allow us to be even more specific. For all three proteins, the type 1 copper ions located in the interior of individual domains and the type 2 copper that is part of the trinuclear cluster have been shown to be most easily removed and reincorporated (8, 50, 53). Moreover, nonradiative tyrosine to tryptophan energy transfer that normally occurs in holo-hCp is not affected by removal of most type 1 and type 2 Cu^{2+} (8, 54), suggesting that these ions play no significant role in the stability of the hCp conformation. Finally, the structure of type 2-depleted laccase from *Coprinus cinereus* displays the canonical pseudo-ternary symmetry with the pair of type 3 copper ions duly positioned at the Nter-Cter interface (41). It is therefore most likely that the pair of type 3 copper ions is primarily responsible for the stabilization of the global protein structure.

Previous spectroscopic studies of apo-hCp were interpreted in terms of a molten globule-like conformation (17), suggesting that the tertiary structure of the protein was significantly altered upon copper removal while the secondary structure was essentially preserved. Our SAXS experiments show that major perturbations following metal removal occur at a higher hierarchical level of structure, that of the mutual arrangement of the pairs of domains. However, the spectroscopic observations can easily be reconciled with the present model. The increase in ANS fluorescence in the absence of copper suggested that significant hydrophobic patches become accessible to the probe (17), an observation that is perfectly compatible with our model. Indeed, whereas we assume that the conformation of individual pairs of domains remains essentially intact, as required by our rigid body analysis, some hydrophobic patches that were buried into the interfaces become accessible to the fluorescence probe. Furthermore, local movements of some parts of the protein destabilized by the removal of copper ions could lead to the transient exposure of hydrophobic residues. The same pattern of conformational modifications can also account for the observed red shift in apo-hCp fluorescence emission spectrum (17). Such spectral change, reporting on a more polar environment experienced by Trp residues, is fully compatible with the extended conformation following the loss of interfaces proposed for apo-hCp. The large number of these residues (18 Trp and 64 Tyr) obviously precludes any site-specific investigation. However, it is worth noting that 5 Trp and 19 Tyr residues appear to be involved in interactions between pairs of domains and are therefore likely to experience an increased exposure to solvent in the apo form.

Mutations in the hCp gene causing expression to stop at residue 991 (55) and 858 (56) have been associated with systemic hemosiderosis. It has already been proposed on the basis of the crystal structure that in such truncated enzymes the trinuclear cluster binding would be affected, thereby severely impairing oxidase activity (13). Furthermore, this could entail a deep enough perturbation of the interface between domains 1 and 6 that the enzyme "may well exist in an open configuration." Our results, showing that this is already the case of the complete enzyme upon copper removal, give a strong experimental support to this proposal.

Rigid-body Dynamics of Holo-hCp—Although the contribution from sugar chains, once properly taken into account, considerably improves the agreement between the calculated and experimental scattering pattern of the holo form of hCp, residual oscillations persist at larger angles, beyond 0.03 $Å^{-1}$, on the calculated pattern (Fig. 3*a*), whatever the number of glycans added. Rotating the hydrocarbon chains around their binding site hardly alters the scattering pattern (data not shown). Therefore, the mobility of the carbohydrate chains cannot account for the smooth appearance of this part of the curve. To remove these oscillations, perturbation of the symmetrical arrangement of the three pairs of domains seems unavoidable. Because the N- and C-terminal pairs of domains are bound at the trinuclear copper site, their mutual movements are restricted, and the required deviation from symmetry can mainly be achieved by assuming the existence of global movements of the central pair of domains with respect to the rest of the molecule. This assumption also follows directly from the previous analysis of the apo-hCp conformation and of the subsequent study of the interfaces between pairs of domains. We have seen that type 1 and type 2 Cu^{2+} are likely to play no significant role in the stability of hCp conformation (8, 54). Therefore, the pairs of domains {1,2} and {5,6} that have been shown to move freely in solution in the case of apo-hCp should not be interacting more strongly with the central pair {3,4} in the presence of copper.

The hypothesis has been put to test by allowing the central pair of domains {3,4} to move as a rigid body with respect to the other two pairs. A significantly improved fit with dampened oscillations beyond 0.02 $Å^{-1}$, identical to the previous curve below 0.018 $Å^{-1}$, was obtained for a displacement of 3 Å along the *x* and *z* axes of the coordinate frame, with rotations between 7 and 40 degrees around the three reference axes (Fig. 3*a*, *light brown line*). The root mean square distance between all Cα is 6.2 Å, whereas the distances between the two positions of the N and C extremities are between 10 and 12 Å, which can be accommodated by the flexibility of the linkers. An even better fit with weaker and shifted oscillations was obtained when the fitting procedure was started from a different initial position (*red line* in Fig. 3*a*). As in the case of the apo form of hCp, the pattern resulting from the motion of the central pair of domains is the average of all accessible conformations weighted by their respective fractional concentration. Averaging a large number of scattering patterns of similarly refined conformations would most likely yield a curve with no detectable modulations. The proposal that the central part of the molecule is already mobile as a whole with respect to the other two pairs of domains within the holoprotein therefore provides an attractive explanation for the absence of oscillations at wider angles observed on the experimental data. In contrast, the quasisymmetric crystal structure appears to be stabilized by packing forces.

CONCLUSION

We have presented here the results of a SAXS study of the conformation in solution of both the holo and apo forms of human ceruloplasmin. The large differences observed between the two scattering patterns show that the protein undergoes a thorough reorganization upon copper removal. An *ab initio* analysis of both curves gives a first hint of the low resolution shapes of the two forms and shows that the pseudo 3-fold symmetry cannot be preserved in the apo form, but a more detailed interpretation entirely relies on the availability of the crystal structure of the holo form. Indeed, the present work fully exploits the fruitful complementarity between high resolution x-ray crystallography and low-resolution SAXS study in solution. The pattern calculated from the crystal structure is different although similar to the experimental data. Modeling the missing parts of the molecule, sugar chains and mobile loops, has improved the fit to the data, but a good agreement is only obtained by introducing a global motion of the central part with respect to the rest of the molecule. Similarly, the observation in the crystal structure of the location of the 3-copper site at the interface between the N-terminal and C-terminal

domains of the protein together with the comparison between the two scattering patterns has led to the proposed model involving the complete loss of the interfaces between the three pairs of domains upon copper removal. Whereas holo-hCp is described in terms of loosely connected pairs of domains, the central one undergoing global motions with respect to the rest of the molecule, the apo form is therefore seen as exploring a large conformational space through rigid-body movements of the pairs of domains around flexible linkers. The comparison between hCp, AO, and laccase provides a structural explanation for the different properties of the three multicopper oxidases in the apo form. In the case of laccase and AO, the contribution from the numerous interactions through tight interfaces and the presence of disulfide bonds preserve the native arrangement of domains in the apo form, thereby allowing for the reversibility of copper removal. In contrast, in the case of hCp, the markedly looser interfaces and the absence of any covalent link yield weak enough interactions that the contribution from the pair of type 3 copper ions to the Nter-Cter interface is indispensable. Upon copper removal, the interface is lost, the two side pairs of domains move apart, the binding site for copper ions is thereupon lost, which explains the observed irreversibility of type 3 copper ions removal in hCp. Our results establish that beyond catalytic activity, the two type 3 copper ions at the N-terminal-C-terminal interface play a crucial role in the structural stability of hCp.

Acknowledgments—We acknowledge the efficient support from the technical staff at LURE-DCI and from the computing center at LURE. We thank A. Jones for bringing to our attention the structure of the Fc fragment with the added glycan chain (PDB 1fc1), A. Roussel for advice with the use of Turbo-FRODO, and F. Rey for critical reading of the manuscript.

REFERENCES

1. Osaki, S., Johnson, D. A., and Frieden, E. (1966) *J. Biol. Chem.* **241,** 2746–2751
2. Osaki, S., Johnson, D. A., and Frieden, E. (1971) *J. Biol. Chem.* **246,** 3018–3023
3. Hellman, N. E., and Gitlin, J. D. (2002) *Annu. Rev. Nutr.* **22,** 439–458
4. Harris, Z. L., Durley, A. P., Man, T. K., and Gitlin, J. D. (1999) *Proc. Natl. Acad. Sci. U. S. A.* **96,** 10812–10817
5. Gutteridge, J. M. C., Richmond, R., and Halliwell, B. (1980) *FEBS Lett.* **112,** 269–272
6. Vassiliev, V. B., Kachurin, A. M., and Soroka, V. N. (1988) *Biochemistry* (*Eng. Transl. Biokimiya*) **53,** 1756–1761
7. Kachurin, A. M., Vassiliev, V. B., and Soroka, V. N. (1989) *Biochemistry* (*Eng. Transl. Biokimiya*) **54,** 26–31
8. Vassiliev, V. B., Kachurin, A. M., Beltramini, M., Rocco, G. P., Salvato, B., and Gaitskhoki, V. S. (1997) *J. Inorg. Biochem.* **65,** 167–174
9. Cha, M. K., and Kim, I. H. (1999) *Biochemistry* **38,** 12104–12110
10. Takahashi, N., Ortel, T. L., and Putnam, F. W. (1984) *Proc. Natl. Acad. Sci. U. S. A.* **81,** 390–394
11. Zaitseva, I., Zaitsev, V., Card, G., Moshkov, K., Bax, B., Ralph, A., and Lindley, P. (1996) *J. Biol. Inorg. Chem.* **1,** 15–23
12. Malmström, B. G. (1978) in *New Trends in Bioinorganic Chemistry* (Williams, R. J. P., and Da Silva, J. R. F., eds) pp. 59–77, Academic Press, New York
13. Lindley, P. F., Card, G., Zaitseva, I., Zaitsev, V., Reinhammar, B., Selin-Lindgren, E., and Yoshida, K. (1997) *J. Biol. Inorg. Chem.* **2,** 454–463
14. Kasper, C. B., and Deutsch, H. F. (1963) *J. Biol. Chem.* **238,** 2325–2337
15. Zakharova, E. T., Vassiliev, V. B., Gorbunova, V. N., and Shavlovski, M. M. (1983) *Biokhimia* **48,** 1709–1720
16. Sato, M., and Gitlin, J. D. (1991) *J. Biol. Chem.* **266,** 5128–5134
17. De Filippis, V., Vassiliev, V. B., Beltramini, M., Fontana, A., Salvato, B., and Gaitskhoki, V. S. (1996) *Biochim. Biophys. Acta* **1297,** 119–123
18. Ptitsyn, O. B. (1995) in *Protein Folding* (Creighton, T. E., ed) pp. 243–300, W. H. Freeman and Co., New York
19. Vachette, P., and Svergun, D. I. (2000) in *Biomolecular Structure and Dynamics* (Fanchon, E., Geissler, E., Hodeau, J. L., Regnard, J. R., and Timmins, P., eds) Vol. IV, pp. 199–237, Oxford University Press, Oxford
20. Fetler, L., Tauc, P., Hervé, G., Moody, M. F., and Vachette, P. (1995) *J. Mol. Biol.* **251,** 243–255
21. Svergun, D. I., Barberato, C., Koch, M. H., Fetler, L., and Vachette, P. (1997) *Proteins* **27,** 110–117
22. Kataoka, M., Hagihara, Y., Mihara, K., and Goto, Y. (1993) *J. Mol. Biol.* **229,** 591–596
23. Segel, D. J., Eliezer, D., Uversky, V., Fink, A. L., Hodgson, K. O., and Doniach, S. (1999) *Biochemistry* **38,** 15352–15359
24. Prozorovski, V. N., Rashkovetski, L. G., Vassiliev, V. B., Shavlovski, M. M., and Neifakh, S. A. (1982) *Int. J. Pept. Protein Res.* **19,** 40–53
25. Gill, S. G., and von Hippel, P. H. (1989) *Anal. Biochem.* **182,** 319–326
26. Boulin, C., Kempf, R., Koch, M. H. J., and McLaughlin, S. M. (1986) *Nucl. Instrum. Methods Sect. A* **249,** 399–407
27. Dubuisson, J. M., Decamps, T., and Vachette, P. (1997) *J. Appl. Cryst.* **30,** 49–54
28. Guinier, A., and Fournet, G. (1955) *Small Angle Scattering of X-rays*, Wiley, New York
29. Svergun, D. I. (1992) *J. Appl. Cryst.* **25,** 495–503
30. Svergun, D. I. (1999) *Biophys. J.* **76,** 2879–2886
31. Feigin, L. A., and Svergun, D. I. (1987) *Structure Analysis by Small-angle X-ray and Neutron Scattering*, Plenum Press, New York
32. Bernstein, F. C., Koetzle, T. F., Williams, G. J., Meyer, E. E., Jr., Brice, M. D., Rodgers, J. R., Kennard, O., Shimanouchi, T., and Tasumi, M. (1977) *J. Mol. Biol.* **112,** 535–542
33. Svergun, D., Barberato, C., and Koch, M. H. J. (1995) *J. Appl. Cryst.* **28,** 768–773
34. Roussel, A., and Cambillau, C. (1989) *Silicon Graphics Geometry Partners Directory,* Silicon Graphics, Mountain View, CA
35. Rydèn, L. (1984) in *Copper Proteins and Copper Enzymes* (Lontie, R., ed) Vol. 3, pp. 37–100, CRC Press, Boca Raton, FL
36. Deisenhofer, J. (1981) *Biochemistry* **20,** 2361–2370
37. Varghese, J. N., Smith, P. W., Sollis, S. L., Blick, T. J., Sahasrabudhe, A., McKimm-Breschkin, J. L., and Colman, P. M. (1998) *Structure* **6,** 735–746
38. Kozin, M. B., Volkov, V. V., and Svergun, D. I. (1997) *J. Appl. Crystallogr.* **30,** 811–815
39. Jones, S., and Thornton, J. M. (1996) *Proc. Natl. Acad. Sci. U. S. A.* **93,** 13–20
40. Messerschmidt, A., Ladenstein, R., Huber, R., Bolognesi, M., Petruzzelli, R., Rossi, A., and Finazzi-Agro, A. (1992) *J. Mol. Biol.* **224,** 179–205
41. Ducros, V., Brzozowski, A. M., Wilson, K. S., Brown, S. H., Oestergaard, P., Schneider, P., Yaver, D. S., Pedersen, A. H., and Davies, G. J. (1998) *Nat. Struct. Biol.* **5,** 310–316
42. Lee, B., and Richards, F. M. (1971) *J. Mol. Biol.* **55,** 379–400
43. Laskowski, R. A. (1991) *J. Mol. Graph.* **13,** 323–330
44. Konarev, P. V., Petoukhov, M. V., and Svergun, D. I. (2001) *J. Appl. Cryst.* **34,** 527–532
45. Gitlin, D., and Janeway, C. A. (1960) *Nature* **185,** 693
46. Matsuda, I., Pearson, T., and Holzmann, N. A. (1974) *Pediatr. Res.* **8,** 821–824
47. Grossmann, J. G., Neu, M., Pantos, E., Schwab, F. J., Evans, R. W., Townes-Andrews, E., Lindley, P. F., Appel, H., Thies, W.-G., and Hasnain, S. S. (1992) *J. Mol. Biol.* **225,** 811–819
48. Svergun, D. I., Petoukhov, M. V., Koch, M. H., and König, S. (2000) *J. Biol. Chem.* **275,** 297–302
49. Savini, I., Morpurgo, L., and Avigliano, L. (1985) *Biochem. Biophys. Res. Commun.* **131,** 25–31
50. Savini, I., D'Alessio, S., Giartosio, A., Morpurgo, L., and Avigliano, L. (1990) *Eur. J. Biochem.* **190,** 491–495
51. Ando, K. (1970) *J. Biochem.* **68,** 501–508
52. Morris, M. C., Hauenstein, B. L. J., and McMillin, D. R. (1983) *Biochim. Biophys. Acta* **743,** 389–393
53. Morpurgo, L., Graziani, M. T., Avigliano, L., Desideri, A., and Mondovi, B. (1981) *Isr. J. Chem.* **21,** 26–29
54. Turoverov, K. K., Rezunkova, O. P., Kuznetsova, I. M., Moshkov, K. A., Borisova, O. P., and Yakovlev, A. S. (1982) *Bioorg. Khim.* **8,** 1165–1172
55. Yoshida, K., Furihata, K., Takeda, S., Nakamura, A., Yamamoto, K., Morita, H., Hiyamuta, S., Ikeda, S., Shimizu, N., and Yanasigawa, N. (1995) *Nat. Genet.* **9,** 267–272
56. Takahashi, Y., Myiajima, H., Shirabe, S., Nagataki, S., Suenaga, A., and Gitlin, J. D. (1996) *Hum. Mol. Genet.* **5,** 81–84